Available online at www.sciencedirect.com

SCIENCE DIRECT

Biochimica et Biophysica Acta 1740 (2005) 499–513

BIOCHIMICA ET BIOPHYSICA ACTA

BBA

http://www.elsevier.com/locate/bba

Progressive left ventricular remodeling, myocyte apoptosis, and protein signaling cascades after myocardial infarction in rabbits ☆

Fuzhong Qin*, Michelle C. Liang, Chang-seng Liang

Cardiology Unit, Department of Medicine, University of Rochester Medical Center, Box 679, 601 Elmwood Avenue, Rochester, NY 14642, USA

Received 21 July 2004; received in revised form 9 November 2004; accepted 16 November 2004
Available online 8 December 2004

Abstract

To determine the temporal changes in oxidative stress, mitogen-activated protein (MAP) kinases and mitochondrial apoptotic proteins, and their relationship to myocyte apoptosis in the remote noninfarcted myocardium after myocardial infarction (MI), rabbits were randomly assigned to either coronary artery ligation to produce MI or sham operation. The animals were sacrificed at 1, 4, 8, or 12 weeks after coronary artery occlusion. Sham rabbits were sacrificed at 12 weeks after surgery. MI rabbits exhibited progressive increases of left ventricular (LV) end-diastolic pressure and end-diastolic dimension, and progressive decreases of LV fractional shortening and dP/dt over 12 weeks. The LV remodeling with LV chamber dilation and LV systolic dysfunction was temporally associated with progressive increases of cardiac oxidative stress as evidenced by decreased myocardial reduced-to-oxidized-glutathione ratio and increased myocardial 8-hydroxydeoxyguanosine and myocyte apoptosis. The ERK and JNK activities were decreased while p38 MAP kinase activity was increased with age of MI. The extent of p38 MAP kinase activation correlated with Bcl-2 phosphorylation. Bcl-2 protein was decreased in both mitochondrial and cytosolic fractions with age of MI. Bax protein was increased in both mitochondrial and cytosolic fractions. Cytochrome c was reduced in mitochondrial fraction and increased in cytosolic fraction in a time-dependent manner after MI. Cleaved caspase 9 and caspase 3 proteins were time-dependently increased after MI. These data suggest that p38 MAP kinase activation is not only time-dependent after MI, but also correlates with oxidative stress, Bcl-2 phosphorylation, and myocyte apoptosis. These changes in the remote noninfarcted myocardium may contribute to LV remodeling and dysfunction after MI.

Keywords: Apoptosis; Infarction; MAP kinase; Mitochondria; Oxygen radical

1. Introduction

Left ventricular (LV) remodeling after myocardial infarction (MI) involves both the infarcted and non-infarcted LV myocardium [1]. Early remodeling as expansion of the infarcted area occurs during acute MI, but overtime, changes also occur in the remote non-infarcted myocardium as evidenced by loss of myocytes, myocyte hypertrophy, and elongation, as well as myocyte slippage and myocardial fibrosis [2], leading to eventual progressive LV dilation and systolic dysfunction [1,2]. Prior studies have shown that myocyte apoptosis occurs in both infarct/peri-infarct and the remote myocardium after MI [3,4]. The extent of apoptosis is greater in the infarct/peri-infarct region in early MI [5]. However, apoptosis increases in a greater proportion in the remote noninfarcted myocardium from 1 to 6 months after MI [5,6], and in patients with chronic ischemic cardiomyopathy [7]. Furthermore, unlike the changes in the peri-infarct region, myocyte apoptosis in the remote noninfarcted myocardium correlates with LV remodeling late post-MI [5,6,8]. These findings suggest that myocyte apoptosis in the remote noninfarcted myocardium contributes significantly to the LV remodeling in chronic ischemic cardiomyopathy. In addition, oxidative stress has been shown to increase in the remote noninfarcted myocardium after MI [2], and plays a

☆ The work was presented in part before in the 2003 Annual Scientific Meeting of the Heart Failure Society of America in Las Vegas, Nevada, September 22, 2003.

* Corresponding author. Tel.: +1 585 275 5209; fax: +1 585 271 2184.
E-mail address: fuzhong_qin@urmc.rochester.edu (F. Qin).

0925-4439/$ - see front matter © 2004 Elsevier B.V. All rights reserved.
doi:10.1016/j.bbadis.2004.11.007

role in the production of apoptosis [9]. Other studies have shown that myocyte apoptosis involves the activation of mitogen-activated protein (MAP) kinases and mitochondrial-mediated apoptotic pathway in myocardial ischemia/reperfusion [10] and end-stage heart failure [11]. However, little is known of the temporal alterations in MAP kinases and mitochondrial-related apoptotic proteins in the remote noninfarcted myocardium after MI. The basis for cross-talk between MAP kinases and mitochondrial-mediated apoptotic pathway remains unclear.

In this study, we proposed to determine the temporal changes in cardiac oxidative stress, MAP kinases and mitochondrial Bcl-2, Bax and cytochrome *c* proteins, and their relationship to myocyte apoptosis in the remote noninfarcted myocardium after MI in rabbits. We also examined the functional role of apoptosis in the remote noninfarcted myocardium in LV remodeling after MI. Cardiac oxidative stress was measured by the ratio of reduced to oxidized glutathione (GSH/GSSG) and immunohistochemistry for 8-hydroxydeoxyguanosine (8-OHdG) staining. The total and phosphorylated forms of MAP kinases, mitochondrial and cytosolic Bcl-2, Bax, and cytochrome *c* proteins were measured by Western blot. Caspase 9 and caspase 3 activities were examined by anti-caspase 9 p10 and anti-cleaved caspase 3 antibodies, respectively. Apoptosis was measured by two independent methods. The standard method using terminal deoxynucleotidyl transferase-mediated dUTP nick end-labeling (TUNEL) detects double-stranded DNA breakage, an event occurring late in apoptosis [12]. The second method utilizing monoclonal antibody against single-stranded DNA (Mab) labeling is more sensitive and detects early apoptotic cells [13].

Here, we found that LV remodeling with chamber dilation and LV dysfunction after MI is temporally associated with cardiac oxidative stress and myocyte apoptosis in myocardium remote from the area of initial ischemic damage. The major new findings of our study are that the phosphorylation of p38 MAP kinase is progressively increased in the remote noninfarcted myocardium after MI and that the activation of p38 MAP kinase correlates with Bcl-2 phosphorylation. The Bcl-2 inactivation and reduction coincides with the release of mitochondrial cytochrome *c* and the activation of caspase 9 and caspase 3. This is also the first report to study the temporal changes in mitochondrial-related apoptotic proteins in animals after MI.

2. Materials and methods

2.1. Animal model and experimental protocol

The study was approved by the University of Rochester Committee on Animal Resources and conformed to the guiding principles approved by the Council of the American Physiological Society and the National Institutes of Health Guide on the humane care and use of laboratory animals.

Healthy adult male New Zealand White rabbits (2.5–3.6 kg, 3 months old) were prepared for MI produced by coronary artery ligation as described before [14]. The animals were anesthetized with intramuscular ketamine (50 mg/kg) and xylazine (2 mg/kg) and artificially ventilated with a respirator (Harvard Apparatus, South Natick, MA). The left thoracotomy and pericardiotomy were performed under isoflurane gas anesthesia. Animals were randomly divided into a sham-operated control group without coronary artery occlusion, or one of the four groups of animals with 1, 4, 8, or 12 weeks of left circumflex coronary artery ligation. In the MI animals, the marginal branch of the left circumflex coronary artery was identified and ligated at the midpoint between the atrioventricular groove and the cardiac apex to produce an infarct area of 28–33% of the left ventricle. Animals were closely monitored after surgery for the development of ascites, respiratory distress, or anorexia, and treated accordingly.

Echocardiograms were taken once a week to assess global LV size and function after MI. At the end of the specified time periods, the animals were prepared for a terminal resting hemodynamic study. The animals were then sacrificed by intravenous sodium pentobarbital (>100 mg/kg). The heart was removed, weighed, and rinsed in ice-cold oxygenated normal saline. The remote noninfarcted myocardium, at least 2 mm away from the margin of the infarct [9], was removed and either used immediately or stored in liquid nitrogen for studies.

2.2. Echocardiographic and hemodynamic measurements

Two-dimensional and M-mode echocardiograms were obtained using a 5-MHz transducer on a Toshiba Model SSH-60A sonographic system (Toshiba America Medical System, Tustin, CA). Maximal LV end-diastolic dimension (EDD) and end-systolic dimension (ESD) were used to calculate LV fractional shortening (FS) by the following equation: FS=[(EDD−ESD)100]/EDD.

For the terminal hemodynamic studies, animals were anesthetized with intramuscular ketamine (35 mg/kg) and midazolam (0.8 mg/kg). A saline-filled catheter was inserted into the left jugular vein. A 20-gauge saline-filled catheter (Insyte; Deseret Medical, Becton Dickinson, Sandy, UT) was introduced into the left carotid artery and connected to a pressure transducer (Model P23XL Spectramed, Oxnard, CA) for measuring aortic pressure. A 2-Fr micromanometer-tipped catheter (Millar Instruments, Houston, TX) was advanced into the left ventricle via the right carotid artery for measuring the LV pressure and the first derivative of the LV pressure rise (dP/dt) using an electronic differentiator. Electrocardiograms, aortic pressure, and the LV dP/dt were recorded on a

Brush Model 480 recorder (Gould, Instruments System Division, Cleveland, OH) and analyzed by an IOX program (EMKA Technologies, Paris, France). Resting hymodynamic measurements were obtained in triplicate over a 20-min steady state period at least a half hour after the catheterization. The averages of triplicates were used for statistical analysis.

2.3. Myocardial infarct size

LV tissue slices were stained at 37 °C for 30 min with 1% triphenyltetrazolium chloride, which stains only the viable myocardium. Infarct size was determined planimetrically as the percentage of unstained left ventricle in the section as described previously [15]. The animals with 28–33% infarct sizes were used in the study.

2.4. Myocardial glutathione measurements

Fresh LV myocardium from the remote noninfarcted region was homogenized in 3 volumes of 1% picric acid and the supernatant collected for measuring total glutathione using a glutathione reductase-coupled enzymatic assay [16] on a Lambda 3 UV/VIS spectrophotometer (Perkin Elmer, Norwalk, CT). Total glutathione was calculated from a standard curve of purified glutathione, and oxidized glutathione (GSSG) was measured by masking the reduced glutathione (GSH) with 2-vinyl pyridine in the enzymatic assay. The ratio of GSH/GSSG was calculated as total tissue oxidative stress.

2.5. Immunohistochemistry for myocardial 8-OHdG

The paraffin sections from the remote noninfarcted region were blocked with 10% horse serum in phosphate-buffered saline (PBS), incubated with goat polyclonal anti-8-OHdG antibody and then incubated with biotin-conjugated anti-goat IgG (Vector Laboratory, Burlingame, CA). The sections were incubated with avidin and biotinylated horseradish peroxidase macromolecular complex (Vector Laboratory), and stained with 3-amino-9-ethylcarbazole (Vector Laboratory) and hematoxylin (Vector Laboratory). For negative control, the primary antibody was omitted. The samples were examined under light microscopy.

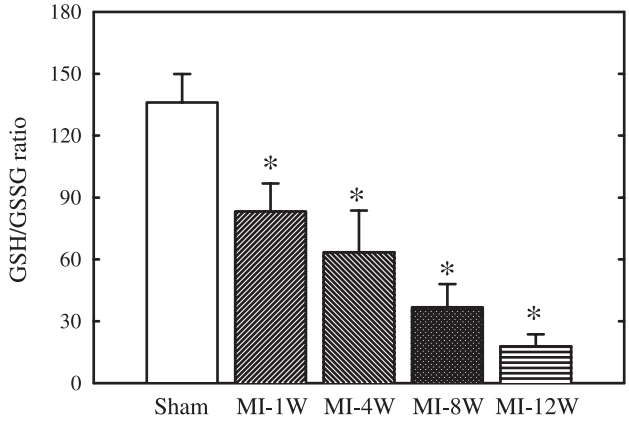

Fig. 1. Changes in myocardial reduced glutathione to oxidized glutathione (GSH/GSSG) ratio in sham and MI rabbits at 1, 4, 8, and 12 weeks after coronary artery ligation. Values are means±S.E., n=8–11. *P<0.05 vs. sham-operated group.

2.6. Preparation of protein extract

For the assay of the MAPKs or phospho-Bcl-2 protein, LV myocardial tissue samples taken from the remote noninfarcted region were washed in ice-cold PBS containing 2.5 mM EDTA, 2 mM β-glycerophosphate, 10 mM NaF, 1 mM Na_3VO_4, and 1 mM phenylmethysulfoyl fluoride and then frozen in liquid nitrogen. The LV myocardial tissue samples were homogenized in the ice-cold homogenization buffer containing 20 mM HEPES (pH

Table 1
Weights and resting hemodynamics in sham and myocardial infarction rabbits

	Sham	MI-1W	MI-4W	MI-8W	MI-12W
Number	10	9	8	8	8
IS (%)	0	30.6±1.4	29.0±2.5	31.0±2.4	30.3±2.2
BW (kg)	3.5±0.1	3.1±0.2	3.2±0.1	3.4±0.1	3.5±0.1
HW (g)	6.8±0.1	6.6±0.2	6.9±0.3	7.3±0.1*	7.8±0.3*
LVW (g)	3.2±0.1	3.1±0.2	3.1±0.1	3.4±0.1	3.7±0.1*
LVW/BW (g/kg)	0.93±0.02	1.00±0.04	0.96±0.03	1.00±0.03*	1.10±0.03*
Lung weight (g)	11.8±0.3	11.7±0.4	14.7±1.3*	14.8±0.9*	14.9±0.9*
Liver weight (g)	84.3±2.7	81.8±3.1	89.1±5.2	89.3±3.5	96.7±3.4*
HR (beats/min)	259±8	273±8	248±10	246±6	238±10*
MABP (mm Hg)	95±4	82±5*	93±1	91±8	86±3*
LVEDP (mm Hg)	7.9±0.7	15.2±0.34*	15.0±1.2*	14.0±1.1*	15.5±2.3*
LVEDD (mm)	15.2±0.1	15.4±0.2	16.8±0.6*	17.7±0.4*	18.3±0.6*
LV dP/dt (mm Hg/s)	4554±181	3998±329*	3845±180*	3679±199*	3021±204*
LV FS (%)	32.1±0.5	28.5±1.4	27.4±1.4*	26.4±1.4*	26.3±0.5*

Values are means±S.E. MI, myocardial infarction; W, week; IS, infarct size; BW, body weight; HW, heart weight; LV, left ventricular; HR, heart rate; MABP, mean aortic blood pressure; EDP, end-diastolic pressure; EDD, end-diastolic dimension; FS, fraction shortening.
* P<0.05, vs. sham-operated group.

7.2), 25 mM NaCl, 2 mM EGTA, 25 mM β-glycerophosphate, 50 mM NaF, 1 mM Na_3VO_4, 0.2 mM dithiothreitol, 1 mM phenylmethysulfoyl fluoride, apotinin (2.2 mg/ml), leupeptin (5 mg/ml). The homogenate was centrifuged at 12,000×*g* for 30 min at 4 °C and the supernatant was collected as protein extracts.

For the determination of protein levels of Bcl-2, Bax, cytochrome *c*, caspase 9, and caspase 3, LV myocardial tissue samples taken from the remote noninfarcted region were homogenized in a lysis buffer containing 1 M Tris–HCl (pH 7.4), 0.25 M sucrose, 0.5 M EDTA (pH 8.0), 100 mM dithiothreitol, 100 mM phenylmethysulfoyl fluoride, apotinin (2.2 mg/ml), leupeptin (5 mg/ml). The homogenate was centrifuged at 12,000×*g* for 30 min at 4 °C and the supernatant was collected as protein extracts.

The protein concentration was determined using the bicinchoninic acid protein assay reagents (Pierce, Rockford, IL).

2.7. Western blotting for MAP kinase proteins and activities

Protein extracts (40–60 μg) were resolved by 10–12% SDS-polyacrylamide gel and transferred to polyvinylidene fluoride membranes. The membranes were blocked in 5% nonfat dry milk in Tris-buffered saline containing 0.05% Tween 20 (TBST) for 1 h at room temperature. The resulting blots were incubated overnight with mouse monoclonal anti-JNK1/2, anti-ERK1/2 or anti-p38 IgG (Santa Cruz Biotechnology, Santa Cruz, CA) to detect total protein levels of JNK1/2, ERK1/2 or p38. The functional activities of JNK, ERK and p38 kinases were determined using phospho-specific antibodies of MAP kinases (p-JNK, p-ERK and p-p38) (Santa Cruz Biotechnology). Mouse anti-β-actin monoclonal antibody (Abcam, Cambridge, MA) was used to confirm equal loading conditions. The dilution for all primary antibodies was 1:200. After the incubation of primary

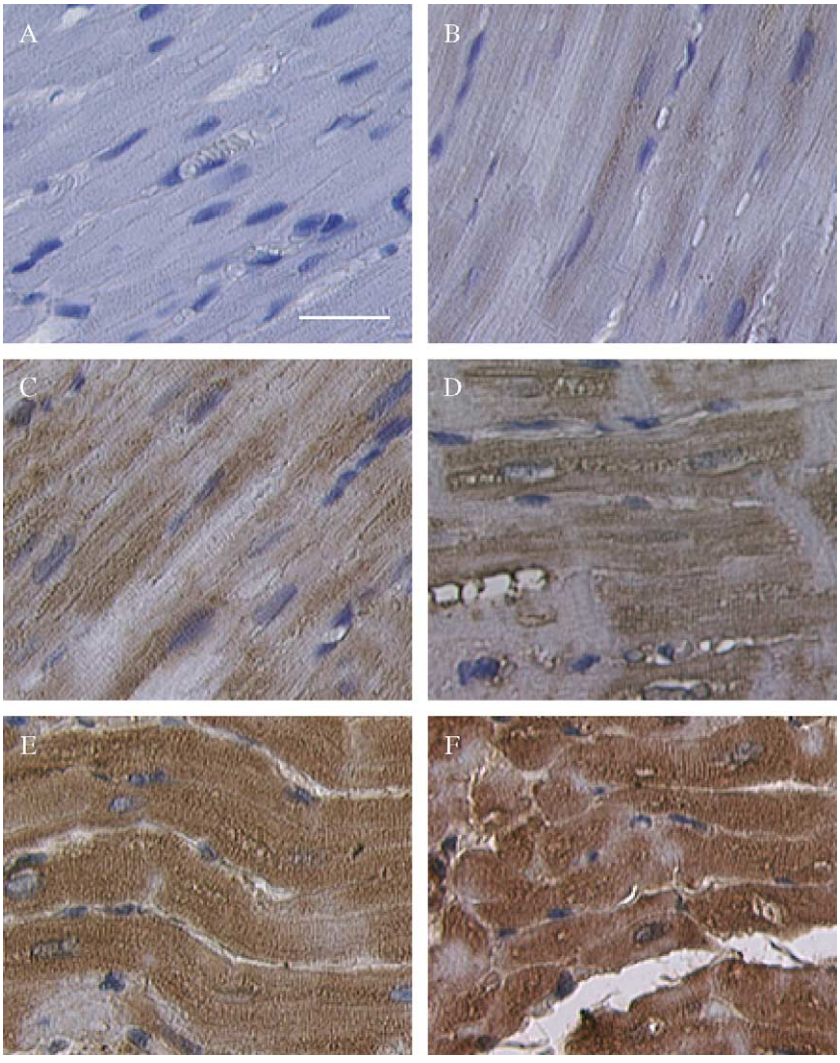

Fig. 2. The photomicrographs of left ventricular tissue sections showing 8-hydroxydeoxygaunosine (8-OHdG) staining. 8-OHdG positive staining is shown red. All nuclei stained by hematoxylin are shown blue. Panel A shows a negative control. Panels B–F show 8-OHdG staining in sham and MI rabbits at 1, 4, 8, and 12 weeks after coronary artery ligation. The positive 8-OHdG stains were increased in MI animals mainly in the cytosol and to lesser extent in the nuclei of the remote noninfarcted myocardial tissue. The bar in panel A indicates 20 μm and accounts for all photomicrographs.

antibodies, blots were washed three times with TBST for 5 min each, incubated with the secondary antibody goat anti-mouse IgG-HRP (1:2000 dilution) for 1 h at room temperature, again followed by three 5-min washes with TBST. The Phototope-HRP Western Blot Detection Kit (Cell Signaling Technology, Beverly, MA) was used to visualize the bands. Autoradiograms were scanned on a Microtek Model 6800 scanner (Microtek Lab, Inc., Carson, CA), and analyzed using the NIH Image 1.60 program. The optical density of tissue samples were normalized to a control sample in an arbitrary densitometry unit.

2.8. Preparation of mitochondrial and cytosolic fractions of myocardial tissue

LV myocardial tissue from the remote noninfarcted region was fractioned into mitochondrial and cytosolic compartments as described previously [17]. In brief, LV myocardial tissue was homogenized and centrifuged at 750×*g* for 10 min at 4 °C and the resultant supernatant was centrifuged at 10,000×*g* for 15 min 4 °C. The pellets containing mitochondrial fraction were resuspended in a storage buffer. The supernatant was further centrifuged at 100,000×*g* for 1 h at 4 °C. The resulting supernatant was used as the cytosolic fraction.

2.9. Determination for phosphorylated Bcl-2, Bcl-2, Bax, and cytochrome c proteins and caspase 9 and 3 activities

Proteins from total tissue extracts, mitochondrial fraction, or cytosolic fraction were separated by 10–12% SDS-polyacrylamide gel and transferred to polyvinylidene fluoride membranes. The membranes were blocked in 5% nonfat dry milk in TBST for 1 h at room temperature. The resulting blots were then incubated overnight with the primary antibodies (1:200 dilution) against phosphorylated Bcl-2 (goat polyclonal anti-phosphorylated-Bcl-2

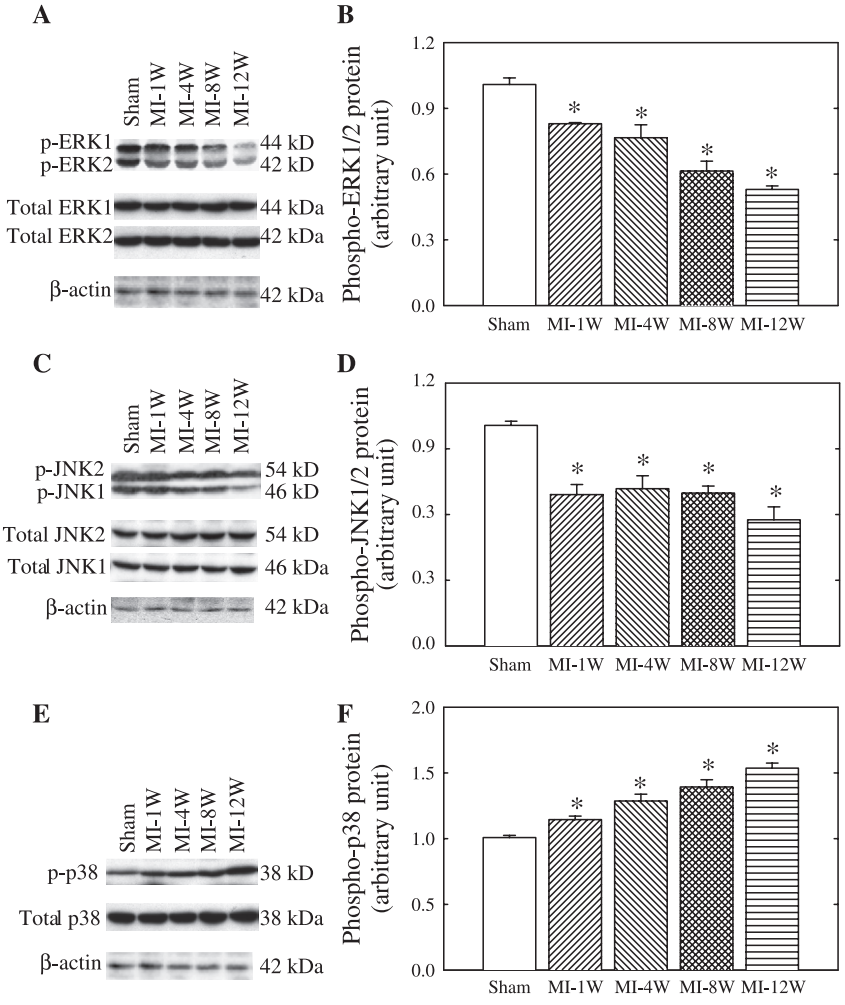

Fig. 3. Changes in phospho-ERK1 and phospho-ERK2 (p-ERK1/2), phospho-JNK1 and phospho-JNK2 (p-JNK1/2), and phospho-p38 MAP kinase (p-p38) proteins in sham and MI rabbits at 1, 4, 8, and 12 weeks after coronary artery ligation. (A, C, E) Representative Western blots of p-ERK1/2 and total ERK1/2, p-JNK1/2 and total JNK1/2, p-p38 and total p38, respectively. Equal loading of proteins is illustrated by β-actin bands. (B, D, F) Respective group densitometry analysis. Values are means±S.E., n=8–11. *P<0.05 vs. sham-operated group. MI, myocardial infarction; W, week.

IgG, Santa Cruz Biotechnology), Bcl-2, Bax, and cytochrome *c* (mouse monoclonal anti-Bcl-2, Bax, and cytochrome *c* IgG, Santa Cruz Biotechnology). Mouse monoclonal anti-caspase 9 (p10) and anti-cleaved caspase 3 antibodies (1:200 dilution) (Cell Signaling Technology) were used to evaluate caspase 9 and caspase 3 activities. Mouse anti-β-actin monoclonal antibody (Abcam; 1:200 dilution) was used to confirm equal loading conditions. After the incubation, blots were washed three times with TBST for 5 min each. The blots were then incubated with the secondary antibody donkey anti-goat IgG-HRP (1:5000 dilution) or goat anti-mouse IgG-HRP (1:2000 dilution) for 1 h at room temperature, again followed by three 5-min washes with TBST. The immunoblotting signals were analyzed as described under Western blotting for MAP kinase proteins and activities.

2.10. TUNEL assay

LV muscle paraffin sections from the remote noninfarcted region were deparaffined, and rehydrated with xylene and graded alcohol series. The sections were stained using the Apoptosis Detection System (Promega, Madison, WI) per the manufacturer's instructions. Briefly, the sections were incubated with terminal deoxynucleotidyl transferase and fluorescein-labeled dUTP. To identify cardiomyocytes, sections were incubated with mouse anti-myosin heavy chain monoclonal antibody (Chemicon International, Temecula, CA). Finally, to identify all nuclei (nonapoptotic and apoptotic), sections were stained with propidium iodide (Sigma-Aldrich, St Louis, MO). The samples were analyzed under a fluorescence microscope. Four sections randomly picked from each of four pieces were analyzed per animal. Cardiomyocyte nuclei were determined by random counting of 10 fields per section. The number of apoptotic nuclei was calculated per 10,000 cardiomyocytes.

2.11. Detection of apoptosis by monoclonal antibody to single-stranded DNA

Frozen tissue sections from the remote noninfarcted region were fixed in 85% methanol in PBS. The sections were incubated with mouse anti-single-stranded DNA monoclonal antibody (Chemicon International). The sections were then incubated with biotin-conjugated anti-mouse IgM (Vector Laboratory) and avidin and biotinylated horseradish peroxidase macromolecular complex

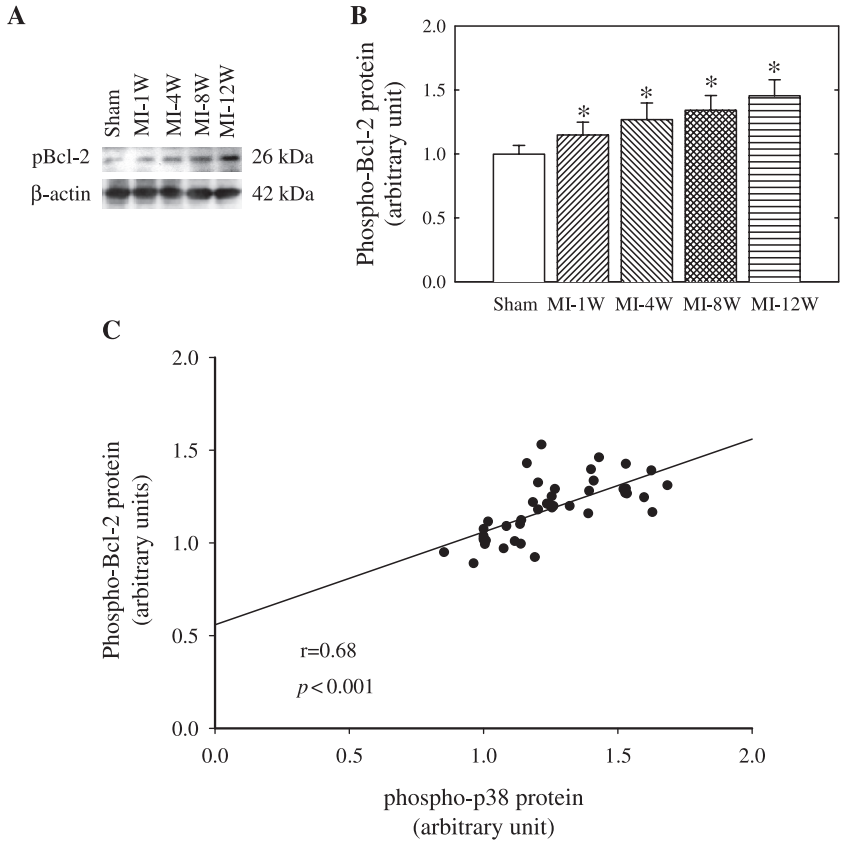

Fig. 4. Changes of phospho-Bcl-2 protein in sham and MI rabbits at 1, 4, 8, and 12 weeks after coronary artery ligation. (A) A representative Western blot of phospho-Bcl-2. Equal loading of proteins is illustrated by β-actin bands. (B) Group densitometry analysis. (C) Correlation between phospho-Bcl-2 protein and phospho-p38 MAP kinase. Values are means±S.E., n=8–11. *P<0.05 vs. sham-operated group. MI, myocardial infarction; W, week.

(Vector Laboratory), and stained with 3-amino-9-ethylcarbazole (Vector Laboratory) and hematoxylin (Vector Laboratory). For the positive control, muscle sections were incubated with proteinase K (20 μg/ml) [18]. The samples were examined under light microscopy. The number of apoptotic nuclei was determined as described in the "TUNEL assay" section.

2.12. Statistical analysis

Results are presented as means±S.E. Student's *t*-test for unpaired data was used to determine the statistical significance of differences between two means. A difference of $P<0.05$ was considered significant. Pearson product-moment correlation coefficient analysis was used to determine the relationship between GSH/GSSG ratio and p38 activity, between p38 activity and Bcl-2 phosphorylation, between myocyte apoptosis (Mab-positive nuclei) and LV EDD, and between myocyte apoptosis and cardiac function (LV FS and LV dP/dt).

3. Results

3.1. Mortality

Nine MI animals died after coronary artery occlusion, yielding an overall mortality rate of 21%. Four rabbits died within 24 h after MI and the other five between day 9 and week 12 after MI. Most deaths were sudden, probably due to

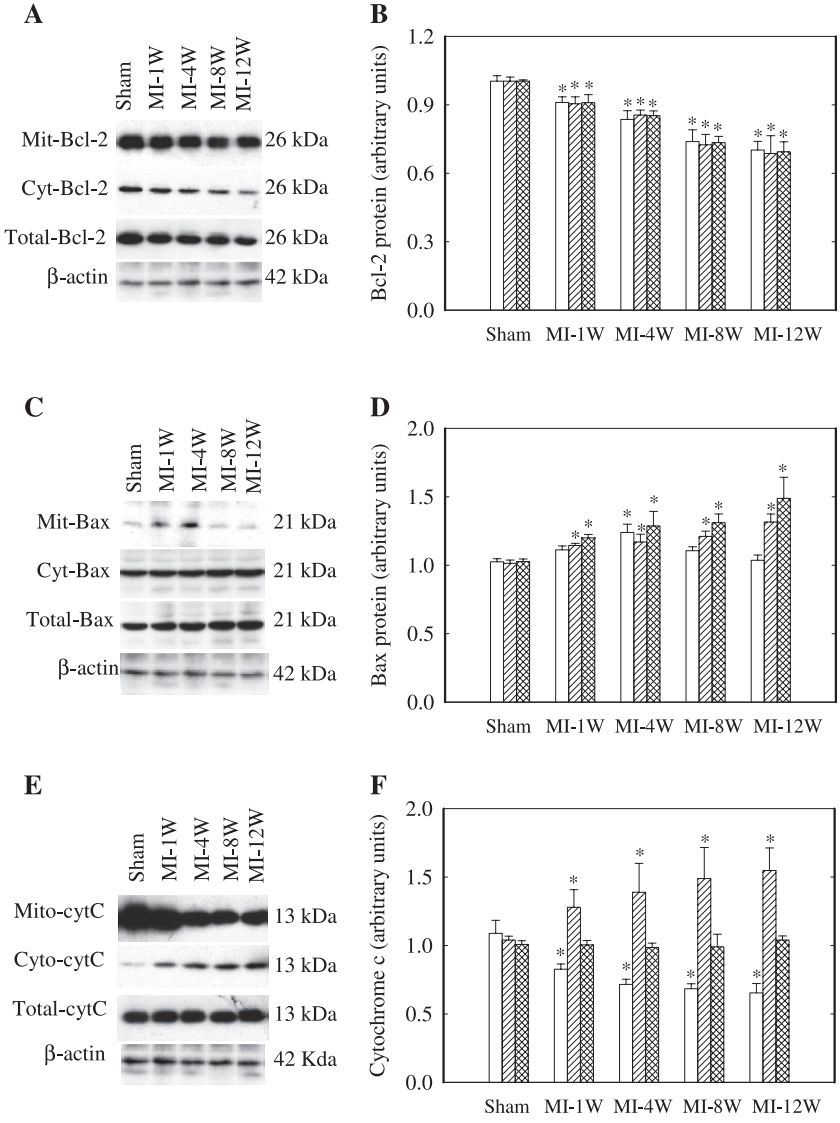

Fig. 5. Changes of Bcl-2, Bax, and cytochrome *c* in mitochondrial fraction, cytosolic fraction, and total tissue homogenate in sham and MI rabbits at 1, 4, 8, and 12 weeks after coronary artery ligation. (A, C, E) Representative Western blots of Bcl-2, Bax, and cytochrome *c*, respectively. Equal loading of proteins is illustrated by β-actin bands. (B, D, F) Respective group densitometry analysis. Values are means±S.E., n=8–11. *$P<0.05$ vs. sham-operated group. MI, myocardial infarction; W, week. Open bar: mitochondrial fraction; hatched bar: cytosolic fraction; cross hatched bar: total tissue homogenate.

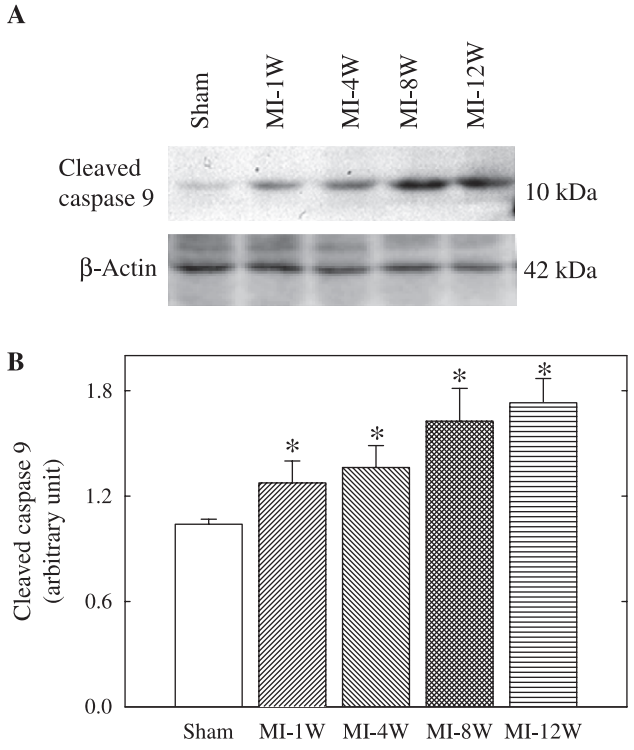

Fig. 6. Changes in cleaved caspase 9 protein in sham and MI rabbits at 1, 4, 8, and 12 weeks after coronary artery ligation. A representative blot of cleaved caspase 9 is shown in panel A. Equal loading of proteins is illustrated by β-actin bands. The group densitometry analysis of cleaved caspase 9 protein is shown in panel B. Values are means±S.E., n=8–11. *P<0.05 vs. sham-operated group. MI, myocardial infarction; W, week.

ventricular fibrillation. None of the sham-operated animals died during the 12-week observation period.

3.2. Cardiac function and resting hemodynamics

Table 1 summarizes the body and heart weights and resting hemodynamics of the Sham and four groups of MI animals. Body weight did not differ significantly among the groups. There was no statistically significant difference in infarct sizes between the four MI groups. Heart weight, LV weight, the ratio of LV weight to body weight, lung weight and liver weight were increased at 12 weeks after MI compared with the Sham. Heart rate and mean aortic blood pressure tended to decrease after MI. MI rabbits exhibited progressive increases of LV end-diastolic pressure and end-diastolic dimension, and progressive decreases of LV fractional shortening and dP/dt over the 12-week period compared with sham animals.

3.3. Myocardial glutathione

Myocardial GSSG content was increased and the ratio of GSH/GSSG decreased in the remote noninfarcted myocardium after MI compared with sham operation, indicating that cardiac oxidative stress was increased in MI animals. The changes appeared to occur in a time-dependent manner (Fig. 1).

3.4. Myocardial 8-OHdG expression

To confirm the increased cardiac oxidative stress after MI, we detected myocardial 8-OHdG, a sensitive and specific marker of DNA damage induced by oxidative stress, using immunohistochemical staining. Fig. 2 shows that the staining intensities of 8-OHdG were stronger in myocardial tissue obtained from MI animals compared with sham-operated animals. As for intracellular localization, positive 8-OHdG stains were increased in MI animals mainly in the cytosol and to lesser extent in the nuclei of the remote noninfarcted myocardial tissue.

3.5. Changes of JNK, ERK, and p38 activities

The phosphorylated active forms of ERK were detected in the rabbit heart as bands corresponding to 44 kDa (p-ERK1) and 42 kDa (p-ERK2). The activity of p-ERK1/2 was decreased over 12-week period in MI rabbits compared with sham animals (Fig. 3A,B). JNK has two phosphorylated active forms detected as 46 kDa (p-JNK1) and 54 kDa (p-JNK2). A decrease of p-JNK1/2 was also found in MI rabbits (Fig. 3C,D). Unlike p-ERK1/2 and p-JNK1/2, p-p38

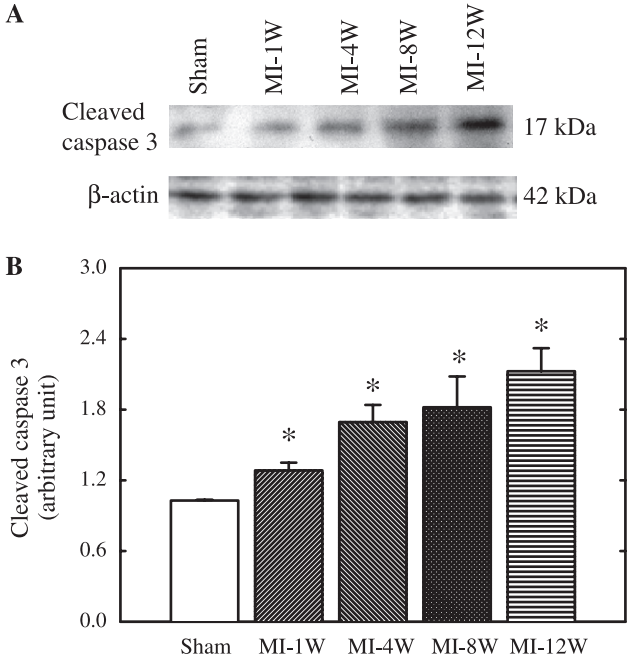

Fig. 7. Changes in cleaved caspase 3 protein in sham and MI rabbits at 1, 4, 8, and 12 weeks after coronary artery ligation. A representative blot of cleaved caspase 3 is shown in panel A. Equal loading of proteins is illustrated by β-actin bands. The group densitometry analysis of cleaved caspase 3 protein is shown in Panel B. Values are means±S.E., n=8–11. *P<0.05 vs. sham-operated group. MI, myocardial infarction; W, week.

increased gradually in MI rabbits in a time-dependent manner (Fig. 3E,F). However, there were no differences in the total protein levels of ERK, JNK and p38 among the sham and MI animals (Fig. 3A,C,E). The uniform appearance of β-actin bands indicates equal protein loading for immunoblotting. The increase in p38 activity correlated with the decrease of GSH/GSSG ratio (r=−0.622, P<0.001).

3.6. Mitochondrial, cytosolic, and total phosphorylated Bcl-2, Bcl-2, Bax, and cytochrome c proteins

To determine whether p38 activation after MI is temporally associated with mitochondrial-mediated apoptotic pathway, we examined the changes in phosphorylated Bcl-2, Bcl-2, Bax, and cytochrome *c* in mitochondrial fraction, cytosolic fraction, or total tissue homogenate. Phosphorylated Bcl-2 protein was progressively increased in MI animals (Fig. 4A,B). The extent of Bcl-2 phosphorylation correlated with p38 activation (Fig. 4C). Bcl-2 protein was decreased in mitochondrial fraction, cytosolic fraction, and total homogenates in MI animals (Fig. 5A,B). Bax protein was slightly increased in mitochondrial fraction at 1 and 4 weeks after MI. A progressive increase of Bax protein was also observed in cytosolic fraction and total homogenates in MI animals (Fig. 5C,D). Studies have shown that Bcl-2 protein inactivation or reduction causes mitochondrial cytochrome *c* release [19]. As expected, cytochrome *c* was

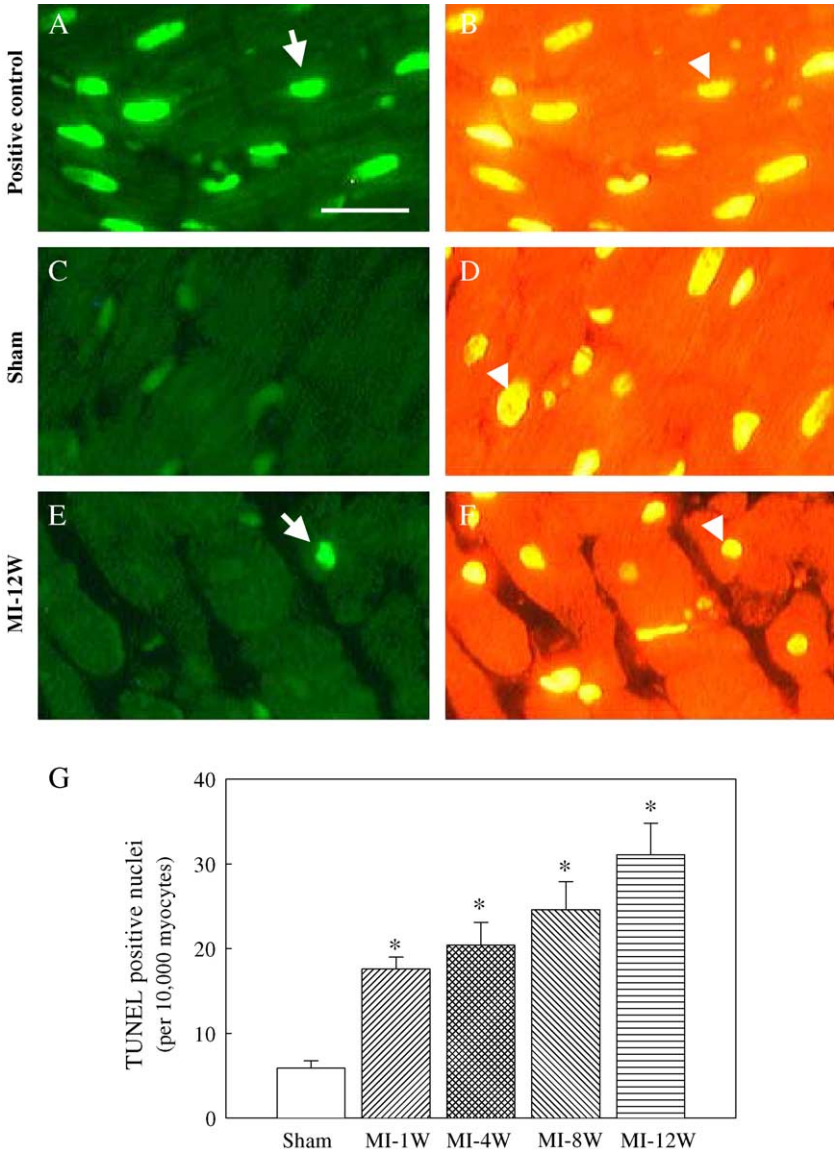

Fig. 8. Photomicrographs of left ventricular tissue sections showing TUNEL staining (A–F). Apoptotic nuclei (arrow) are shown by green fluorescence in panels A, C, and E. The localization of nuclei is documented by propidium iodide staining (arrowhead) and peripheral distribution of β-heavy chain antibody labeling of myocyte cytoplasm illustrated by red fluorescence in panels B, D, and F. The group data are shown in panel G. Values are means±S.E., n=8–11. *P<0.05 vs. sham-operated group. MI, myocardial infarction; W, week. The bar in panel A indicates 20 μm and accounts for all photomicrographs.

reduced in mitochondrial fraction and increased in cytosolic fraction in MI animals compared with sham operation (Fig. 5E,F). These changes appeared a time-dependent manner.

3.7. Cleaved caspase 9 and 3 proteins

To determine whether caspase 9 and caspase 3 were activated, we detected the cleaved proteins of caspase 9 and caspase 3 by immunoblotting. Procaspase 9 exists as a 45-kDa inactive precursor that is cleaved proteolytically to the active subunits p35 and p10. Fig. 6A shows a representative blot of the active subunit p10 of myocardial caspase 9 as detected by a monoclonal anti-caspase 9 p10 antibody. Densitometric analysis indicates that the active caspase 9 was time-dependently elevated in MI rabbits (Fig. 6B). Caspase 3 normally exists as a 32-kDa inactive precursor that is cleaved proteolytically to an active p17 subunit when cells are induced to undergo apoptosis. Fig. 7A shows a representative blot of the 17-kDa subunit of myocardial caspase 3 as detected by a cleaved caspase 3 antibody. The active caspase 3 was increased with time in MI rabbits compared with sham rabbits (Fig. 7B).

3.8. Myocyte apoptosis measured by TUNEL assay

Fig. 8 shows the TUNEL staining in remote myocardial tissue. The specificity of the technique to detect DNA fragmentation was documented by positive labeling of nuclei after exposure of the tissue to DNase I (Fig. 8A,B). DNA fragmentation was not detected when the terminal deoxynucleotidyl transferase was omitted in the enzymatic reaction (data not shown). Identification of apoptotic cardiomyocytes was confirmed by double labeling of cells in which the fragmented DNA and ventricular myosin β-heavy chain were co-localized in the same cell. Representative pictures of the TUNEL staining from a sham and a 12-week MI animal are shown in Fig. 8C–F. Fig. 8G shows that as a group, the number of TUNEL-positive nuclei was significantly increased in the remote myocardium in animals with age of MI.

3.9. Myocyte apoptosis detected by Mab to single-stranded DNA

The specificity of the immunohistochemical staining of single-stranded DNA by Mab in apoptotic cardiomyocytes was documented in tissue sections after exposure to proteinase K (Fig. 9A). No staining was detected when Mab was omitted (data not shown). Representative pictures of the Mab staining from a Sham and a 12-week MI rabbit are shown in Fig. 9B,C. The number of Mab-positive cells increased progressively over the 12-week period in MI rabbits (Fig. 9D). The number of Mab-positive cells was greater than that detected by TUNEL staining in the same tissue.

3.10. Correlation of myocyte apoptosis with LV diameter and function after MI

There was a positive correlation between myocyte apoptosis and LV EDD (Fig. 10A). Significant negative

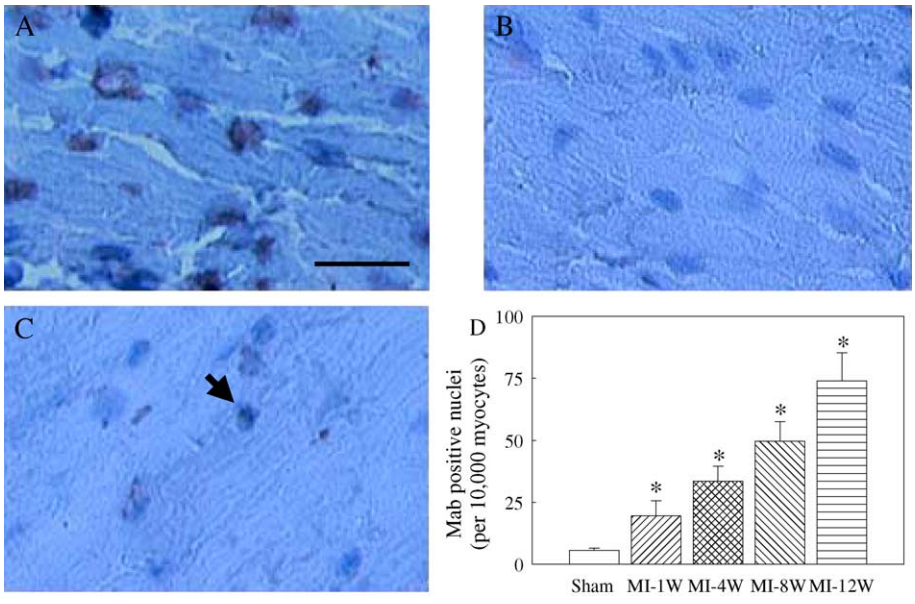

Fig. 9. Photomicrographs of rabbit left ventricular tissue sections showing Mab staining (A–C). The Mab-stained nuclei are shown brownish. Other nuclei stained by hematoxylin alone are shown blue. Panel A illustrates positive control with multiple Mab-positive nuclei after proteinase K treatment. The Mab staining of the tissue sections obtained from a sham and a 12-week MI rabbit are shown in panels B and C, respectively. The group data are shown in panel D. Values are means±S.E., n=8–11. *P<0.05 vs. sham-operated group. MI, myocardial infarction; W, week. The bar in panel A indicates 20 μm and accounts for all photomicrographs.

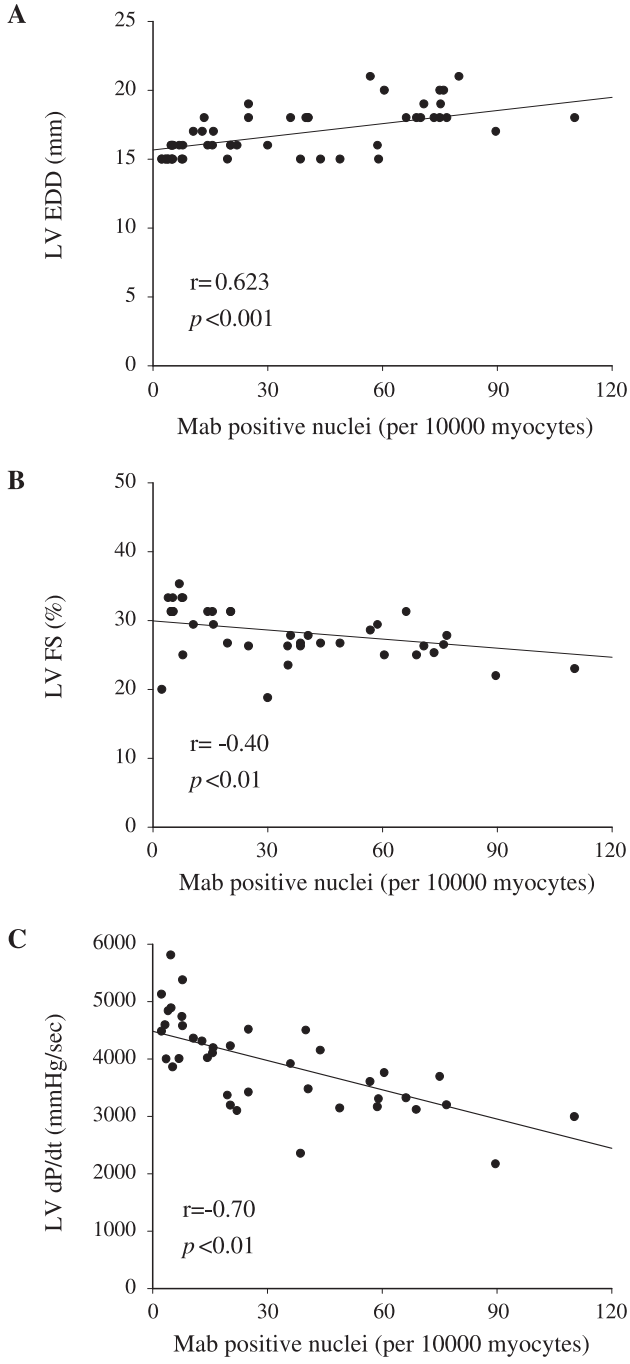

Fig. 10. Correlations between myocyte apoptosis and LV end-diastolic dimension (A), and between myocyte apoptosis and cardiac function (LV fractional shortening and LV d*P*/d*t*, panels B and C). Each data point represents one animal. EDD: end-diastolic dimension. FS: fractional shortening. *r*: coefficient of correlation.

correlation was observed between myocyte apoptosis and cardiac function (LV FS and LV d*P*/d*t*) (Fig. 10B,C). The correlations suggest that the extent of myocyte apoptosis in the remote myocardium may be an important factor in determining the degree of cardiac dilation and LV dysfunction after MI.

4. Discussion

Results of our present study indicate that MI rabbits exhibited progressive increases of LV end-diastolic pressure and end-diastolic dimension, and decreases of LV fractional shortening and d*P*/d*t* over 12 weeks after MI. The LV remodeling with chamber dilation and LV systolic dysfunction was temporally associated with increases of cardiac oxidative stress measured by GSH/GSSG ratio and a new marker myocardial 8-OHdG and myocyte apoptosis in myocardium remote from the area of initial ischemic damage. Furthermore, we showed a progressive increase of p38 MAP kinase phosphorylation after MI and a correlation of active p38 MAP kinase with Bcl-2 phosphorylation. The change in Bcl-2 protein coincided temporally with the release of mitochondrial cytochrome *c* and the activation of caspase 9 and caspase 3.

4.1. Oxidative stress in the remote noninfarcted myocardium

Previous studies have shown that oxidative stress, determined by the level of lipid peroxidation, is increased in the remote noninfarcted myocardium after MI in rats and that the increase is prevented by the treatment of probucol [20] or a combination of probucol and pyrrolidine dithiocarbamate [21]. This is consistent with our present study showing that oxidative stress as assessed by GSH/GSSG ratio and a new marker myocardial 8-OHdG is increased in the remote noninfarcted myocardium in rabbits. The oxidative stress is probably derived from multiple sources of reactive oxygen species. First, the chronic hemodynamic stress after MI may lead to an unrelenting up-regulation of oxidative metabolism in the surviving myocardium and, causes a sustained increase in the production of mitochondrial derived oxygen free radicals [21]. Stretch as the heart dilates also has been shown to increase superoxide radical production in the myocardium [22]. Second, hydroxyl radicals, generated from superoxide anion, and lipid peroxide formation in the mitochondria, are increased in the noninfarcted myocardium after MI [23]. Third, neurohumoral activation known to occur in ischemic cardiomyopathy can also increase reactive oxygen species in the noninfarcted myocardium via production of oxidative metabolites of catecholamines and angiotensin II-medicated NADPH oxidase activation. More recently, xanthine oxidoreductase is identified as another important source of cardiac oxygen free radicals. Xanthine oxidoreductase activity is increased in the myocardium after MI, indicating that increased xanthine oxidoreductase activity may contribute to increased oxidative stress in the remote noninfarcted myocardium [24]. We speculate that the increased oxidative stress in the noninfarcted myocardium plays an important role in the production of cardiac dysfunction and LV remodeling after MI. This is supported by the findings that probucol and dimethylthiourea, which reduce oxidative stress in the

remote noninfarted myocardium, improve LV remodeling after MI [20,25,26].

4.2. Oxidative stress and MAP kinases

Growing evidence has shown that oxidative stress increases after MI [27]. Increased oxidative stress may activate multiple cell signaling pathways, including the MAP kinase pathways, and contribute to the progression of LV remodeling and failure after MI [26]. Oxidative stress has been shown to activate all three MAP kinase subfamilies in neonatal rat ventricular myocytes [28,29] and isolated perfused rat hearts [30]. It is also responsible for p38 phosphorylation of the heart in intact animals after ischemia and reperfusion [31]. In our present study, we observed differential activation of myocardial MAP kinases in the remote noninfarcted myocardium after MI. The activities of ERK and JNK were decreased 1 week after MI and remained lower thereafter, while p38 activity increased progressively with time after MI. We further found that the increase in p38 activity was associated with increased oxidative stress in the remote noninfarcted myocardium after MI.

4.3. MAP kinases and myocyte apoptosis

MAP kinases have been shown to play an important role in the regulation of cell growth and apoptosis [32]. The dynamic balance among the effects of ERK, JNK, and p38 is important in determining whether a cell will survive or undergo apoptosis [32]. Activation of ERK causes cardiac hypertrophy and increases survival, while inactivation of ERK contributes to myocyte apoptosis. This is supported by recent studies showing that inhibition of ERK enhances ischemia/reoxygenation-induced apoptosis in cultured cardiac myocytes [33] and that the decrease of ERK activity mediated by oxidative stress coincides with myocyte apoptosis in heart failure [34]. The decreased activity of ERK in the remote noninfarcted myocardium of MI animals may play a role in myocyte apoptosis in our study. Previous studies have also implicated a pro-apoptotic role of activated JNK [35]. JNK activation is found in the failing human ischemic hearts [36] and the active JNK is associated with oxidative stress and myocyte apoptosis after large MI in rats [9]. In our present study, JNK activity was decreased in the remote noninfarcted myocardium after MI. Our present findings, however, are not unique, because inactivation of JNK also was found in the failing human hearts [37]. It is possible that JNK is inactivated by negative feedback regulation of the increased MAP kinase phosphatase 1/2 in the failing hearts [37]. This notion is supported by the recent observation that overexpression of MAP kinase phosphatase 1 inhibits oxidative stress-induced JNK activity and apoptosis [38].

Unlike the changes in ERK and JNK activities, a progressive increase of p38 activity was observed in the remote noninfarcted myocardium after MI in our present study. Activation of p38 was also found after myocardial ischemia and reperfusion [10,31]. Inhibition of oxidative stress-mediated p38 activation attenuates infarct size and myocyte apoptosis after myocardial ischemia and reperfusion [31]. Activation of p38 by oxidative stress in neonatal ventricular myocytes also has been shown to induce myocyte apoptosis [29]. In addition, activation of p38 decreases H_2O_2-induced ERK activation in cardiac myocytes, indicating a cross-talk mechanism between p38 and ERK signaling pathways for modulation of apoptosis during oxidative stress [39]. In our present study, the decrease of ERK activity occurred with activation of p38 in the remote noninfarcted myocardium after MI. These findings collectively suggest that p38 activation may play an important role in myocyte apoptosis after MI.

4.4. P38 activation, Bcl-2 phosphorylation, and mitochondrial cytochrome c release

The family of Bcl-2-related proteins constitutes a class of apoptosis-regulatory gene products. Anti-apoptotic Bcl-2 is predominately located to the outer-mitochondrial membrane. In contrast, the majority of proapoptotic Bax is located in cytosol in monomeric inactive form. Upon apoptosis induction, cytosolic Bax translocates from the cytosol to the mitochondria on activation while Bcl-2 phosphorylation or reduction loses its antiapoptotic function [19,40]. In the present study, we found that phosphorylated Bcl-2 was increased with the time after MI. This increase of phosphorylation of Bcl-2 indicates the loss of antiapoptotic function. Moreover, Bcl-2 protein was progressively decreased in mitochondria and cytosol, along with a corresponding increase of cytosolic Bax protein after MI. We have further shown that the phosphorylation of Bcl-2 correlated with p38 activation after MI. The close association between p38 activation and Bcl-2 phosphorylation has been shown previously in the cultured lymphoblastoid cells [41] and neuronal cells [42]. The targeted inhibition of p38 also has been shown to promote up-regulation of Bcl-2 in the hearts of transgenic mice [43]. In contrast, expression of an activated p38 mutant down-regulates Bcl-2 protein levels in the cultured neonatal cardiomyocytes [43]. A recent study also showed that the phosphorylation of p38 induced by oxidative stress was linked to mitochondrial apoptotic pathway in neurons [44]. These findings suggest that p38 phosphorylation is closely related to the changes in Bcl-2. Furthermore, since Bcl-2 protein inhibits mitochondrial cytochrome *c* release, we suspect that the activation of p38 and decrease of Bcl-2 in the remote noninfarcted myocardium after MI may be fundamentally important in mediating the release of cytochrome *c* to the cytoplasm, activation of caspase 9 and caspase 3, and myocyte apoptosis. However, our present study provides no direct proof; further experiments are needed to establish the causal role of p38 activation in

the changes of Bcl-2 and Bax and release of cytochrome *c* in cardiomyocytes.

4.5. Myocyte apoptosis and LV remodeling after MI

LV remodeling is characterized by progressive chamber dilation and systolic/diastolic dysfunction after MI. The process involves cellular and molecular mechanisms both at the site of infarction and the surviving unaffected area [45]. The number of myocytes is reduced in the infarcted heart, but the heart is dilated and hypertrophied, because of compensatory myocyte hypertrophy, myocardial fibrosis, and mural slippage of cardiac cells [46]. Myocyte apoptosis occurs in central ischemic myocardium and border zone 24 h post MI [7,47]. Myocyte apoptosis has also been shown to increase in the noninfarcted myocardium from 1 to 12 weeks post MI in rats [7]. The amount of apoptosis in remote myocardium correlates with an increase in the ventricular diameter 1 and 4 weeks after MI [7]. This suggests that myocyte apoptosis in this region plays a role in the post-MI ventricular remodeling. Furthermore, a long-term observation shows a progressive increase in the number of myocyte apoptosis from 1 to 6 month post MI in mice [5]. The increased myocyte apoptosis in the noninfarcted myocardium is temporally associated with chronic LV remodeling after MI. Our present study showed a positive correlation between the number of myocyte apoptosis in the remote noninfarcted myocardium and LV dilation and dysfunction after MI in rabbits. Similarly, high numbers of apoptotic myocytes are associated with LV dilation in patients with post-infarction heart failure [48], progressive ventricular dysfunction post MI [8], and the clinical severity of deterioration in human dilated cardiomyopathy [49]. Furthermore, as caspases are the key effector molecules for apoptosis, long-term caspase inhibition has been shown to reduce myocyte apoptosis and LV dilation after MI [50]. Targeted deletion of caspase 1 reduces LV dilation following MI [51]. These findings suggest that myocyte apoptosis may represent an important mechanism contributing to progressive myocyte loss, LV dilation and dysfunction after MI.

4.6. Perspectives

Results of our study indicate that p38 is progressively activated in the remote noninfarcted myocardium over a 12-week period after MI. The activation of p38 correlates with increased cardiac oxidative stress and Bcl-2 phosphorylation. The temporal change in Bcl-2 protein also coincides with the release of mitochondrial cytochrome *c*, activation of caspase 9 and caspase 3, and myocyte apoptosis. We speculate that this sequence of events in cardiac oxidative stress, protein signaling cascades, and myocyte apoptosis after MI is pathophysiologically important in the progression of LV remodeling after MI. However, further studies are needed to establish the direct causal effect of p38 activation on Bcl-2 phosphorylation, myocyte apoptosis in the remote noninfarcted myocardium, and LV remodeling late after MI. The functional importance of oxidative stress in myocyte apoptosis in remote noninfarcted myocardium and LV remodeling after MI shall also be studied using antioxidants or free radical scavengers.

Acknowledgements

The study was supported in part by an American Heart Association Scientist Development Grant and USPHS grant #HL-68151.

References

[1] S. Hayashidani, H. Tsutsui, M. Ikeuchi, T. Shiomi, H. Matsusaka, T. Kubota, K. Imanaka-Yoshida, T. Itoh, A. Takeshita, Targeted deletion of MMP-2 attenuates early LV rupture and late remodeling after experimental myocardial infarction, Am. J. Physiol. Heart Circ. Physiol. 285 (2003) H1229–H1235.

[2] W.G. Li, A. Zaheer, L. Coppey, H.J. Oskarsson, Activation of JNK in the remote myocardium after large myocardial infarction in rats, Biochem. Biophys. Res. Commun. 246 (1998) 816–820.

[3] S. Bialik, D.L. Geenen, I.E. Sasson, R. Cheng, J.W. Horner, S.M. Evans, E.M. Lord, C.J. Koch, R.N. Kitsis, Myocyte apoptosis during acute myocardial infarction in the mouse localizes to hypoxic regions but occurs independently of p53, J. Clin. Invest. 100 (1997) 1363–1372.

[4] Q. Li, B. Li, X. Wang, A. Leri, K.P. Jana, Y. Liu, J. Kajstura, R. Baserga, P. Anversa, Overexpression of insulin-like growth factor-1 in mice protects from myocyte death after infarction, attenuating ventricular dilation, wall stress, and cardiac hypertrophy, J. Clin. Invest. 100 (1997) 1991–1999.

[5] E. Palojoki, A. Saraste, A. Eriksson, K. Pulkki, M. Kallajoki, L.M. Voipio-Pulkki, I. Tikkanen, Cardiomyocyte apoptosis and ventricular remodeling after myocardial infarction in rats, Am. J. Physiol. Heart Circ. Physiol. 280 (2001) H2726–H2731.

[6] F. Sam, D.B. Sawyer, D.L. Chang, F.R. Eberli, S. Ngoy, M. Jain, J. Amin, C.S. Apstein, W.S. Colucci, Progressive left ventricular remodeling and apoptosis late after myocardial infarction in mouse heart, Am. J. Physiol. Heart Circ. Physiol. 279 (2000) H422–H428.

[7] G. Olivetti, R. Abbi, F. Quaini, J. Kajstura, W. Cheng, J.A. Nitahara, E. Quaini, C. Di Loreto, C.A. Beltrami, S. Krajewski, J.C. Reed, P. Anversa, Apoptosis in the failing human heart, N. Engl. J. Med. 336 (1997) 1131–1141.

[8] A. Baldi, A. Abbate, R. Bussani, G. Patti, R. Melfi, A. Angelini, A. Dobrina, R. Rossiello, F. Silvestri, F. Baldi, G. Di Sciascio, Apoptosis and post-infarction left ventricular remodeling, J. Mol. Cell. Cardiol. 34 (2002) 165–174.

[9] W.G. Li, L. Coppey, R.M. Weiss, H.J. Oskarsson, Antioxidant therapy attenuates JNK activation and apoptosis in the remote noninfarcted myocardium after large myocardial infarction, Biochem. Biophys. Res. Commun. 280 (2000) 353–357.

[10] X.L. Ma, S. Kumar, F. Gao, C.S. Louden, B.L. Lopez, T.A. Christopher, C. Wang, J.C. Lee, G.Z. Feuerstein, T.L. Yue, Inhibition of p38 mitogen-activated protein kinase decreases cardiomyocyte apoptosis and improves cardiac function after myocardial ischemia and reperfusion, Circulation 99 (1999) 1685–1691.

[11] J. Narula, P. Pandey, E. Arbustini, N. Haider, N. Narula, F.D. Kolodgie, B. Dal Bello, M.J. Semigran, A. Bielsa-Masdeu, G.W. Dec, S. Israels, M. Ballester, R. Virmani, S. Saxena, S. Kharbanda, Apoptosis in heart failure: release of cytochrome *c* from mitochondria

and activation of caspase-3 in human cardiomyopathy, Proc. Natl. Acad. Sci. U. S. A. 96 (1999) 8144–8149.
[12] I. Watanabe, M. Toyoda, J. Okuda, T. Tenjo, K. Tanaka, T. Yamamoto, H. Kawasaki, T. Sugiyama, Y. Kawarada, N. Tanigawa, Detection of apoptotic cells in human colorectal cancer by two different in situ methods: antibody against single-stranded DNA and terminal deoxynucleotidyl transferase-mediated dUTP-biotin nick end-labeling (TUNEL) methods, Jpn. J. Cancer Res. 90 (1999) 188–193.
[13] O.S. Frankfurt, J.A. Robb, E.V. Sugarbaker, L. Villa, Monoclonal antibody to single-stranded DNA is a specific and sensitive cellular marker of apoptosis, Exp. Cell Res. 226 (1996) 387–397.
[14] G.D. Pennock, D.D. Yun, P.G. Agarwal, P.H. Spooner, S. Goldman, Echocardiographic changes after myocardial infarction in a model of left ventricular diastolic dysfunction, Am. J. Physiol. Heart Circ. Physiol. 273 (1997) H2018–H2029.
[15] P.J. Fletcher, J.M. Pfeffer, M.A. Pfeffer, E. Braunwald, Left ventricular diastolic pressure–volume relations in rats with healed myocardial infarction. Effects on systolic function, Circ. Res. 49 (1981) 618–626.
[16] O.W. Griffith, Determination of glutathione and glutathione disulfide using glutathione reductase and 2-vinylpyridine, Anal. Biochem. 106 (1980) 207–212.
[17] S. Phaneuf, C. Leeuwenburgh, Cytochrome *c* release from mitochondria in the aging heart: a possible mechanism for apoptosis with age, Am. J. Physiol., Regul. Integr. Comp. Physiol. 282 (2002) R423–R430.
[18] O.S. Frankfurt, J.A. Robb, E.V. Sugarbaker, L. Villa, Apoptosis in breast carcinomas detected with monoclonal antibody to single-stranded DNA: relation to bcl-2 expression, hormone receptors, and lymph node metastases, Clin. Cancer Res. 3 (1997) 465–471.
[19] B.P. Kang, S. Frencher, V. Reddy, A. Kessler, A. Malhotra, L.G. Meggs, High glucose promotes mesangial cell apoptosis by oxidant-dependent mechanism, Am. J. Physiol., Renal. Physiol. 284 (2003) F455–F466.
[20] Y.T. Sia, T.G. Parker, P. Liu, J.N. Tsoporis, A. Adam, J.L. Rouleau, Improved post-myocardial infarction survival with probucol in rats: effects on left ventricular function, morphology, cardiac oxidative stress and cytokine expression, J. Am. Coll. Cardiol. 39 (2002) 148–156.
[21] H.J. Oskarsson, L. Coppey, R.M. Weiss, W.G. Li, Antioxidants attenuate myocyte apoptosis in the remote non-infarcted myocardium following large myocardial infarction, Cardiovasc. Res. 45 (2000) 679–687.
[22] W. Cheng, B. Li, J. Kajstura, P. Li, M.S. Wolin, E.H. Sonnenblick, T.H. Hintze, G. Olivetti, P. Anversa, Stretch-induced programmed myocyte cell death, J. Clin. Invest. 96 (1995) 2247–2259.
[23] T. Ide, H. Tsutsui, S. Hayashidani, D. Kang, N. Suematsu, K. Nakamura, H. Utsumi, N. Hamasaki, A. Takeshita, Mitochondrial DNA damage and dysfunction associated with oxidative stress in failing hearts after myocardial infarction, Circ. Res. 88 (2001) 529–535.
[24] J.W. de Jong, R.G. Schoemaker, R. de Jonge, P. Bernocchi, E. Keijzer, R. Harrison, H.S. Sharma, C. Ceconi, Enhanced expression and activity of xanthine oxidoreductase in the failing heart, J. Mol. Cell. Cardiol. 32 (2000) 2083–2099.
[25] Y.T. Sia, N. Lapointe, T.G. Parker, J.N. Tsoporis, C.F. Deschepper, A. Calderone, A. Pourdjabbar, J.F. Jasmin, J.F. Sarrazin, P. Liu, A. Adam, J. Butany, J.L. Rouleau, Beneficial effects of long-term use of the antioxidant probucol in heart failure in the rat, Circulation 105 (2002) 2549–2555.
[26] S. Kinugawa, H. Tsutsui, S. Hayashidani, T. Ide, N. Suematsu, S. Satoh, H. Utsumi, A. Takeshita, Treatment with dimethylthiourea prevents left ventricular remodeling and failure after experimental myocardial infarction in mice: role of oxidative stress, Circ. Res. 87 (2000) 392–398.
[27] D. Kumar, H. Lou, P.K. Singal, Oxidative stress and apoptosis in heart dysfunction, Herz 27 (2002) 662–668.
[28] R. Aikawa, I. Komuro, T. Yamazaki, Y. Zou, S. Kudoh, M. Tanaka, I. Shiojima, Y. Hiroi, Y. Yazaki, Oxidative stress activates extracellular signal-regulated kinases through Src and Ras in cultured cardiac myocytes of neonatal rats, J. Clin. Invest. 100 (1997) 1813–1821.
[29] A. Clerk, A. Michael, P.H. Sugden, Stimulation of multiple mitogen-activated protein kinase sub-families by oxidative stress and phosphorylation of the small heat shock protein. HSP25/27, in neonatal ventricular myocytes, Biochem. J. 333 (1998) 581–589.
[30] A. Clerk, S.J. Fuller, A. Michael, P.H. Sugden, Stimulation of "stress-regulated" mitogen-activated protein kinases (stress-activated protein kinases/c-Jun N-terminal kinases and p38-mitogen-activated protein kinases) in perfused rat hearts, J. Biol. Chem. 273 (1998) 7228–7234.
[31] K. Kato, H. Yin, J. Agata, H. Yoshida, L. Chao, J. Chao, Adrenomedullin gene delivery attenuates myocardial infarction and apoptosis after ischemia and reperfusion, Am. J. Physiol. Heart Circ. Physiol. 285 (2003) H1506–H1514.
[32] Z. Xia, M. Dickens, J. Raingeaud, R.J. Davis, M.E. Greenberg, Opposing effects of ERK and JNK-p38 MAP kinases on apoptosis, Science 270 (1995) 1326–1331.
[33] T.L. Yue, C. Wang, J.L. Gu, X.L. Ma, S. Kumar, J.C. Lee, G.Z. Feuerstein, H. Thomas, B. Maleeff, E.H. Ohlstein, Inhibition of extracellular signal-regulated kinase enhances ischemia/reoxygenation-induced apoptosis in cultured cardiac myocytes and exaggerates reperfusion injury in isolated perfused heart, Circ. Res. 86 (2000) 692–699.
[34] F. Qin, J. Shite, C.S. Liang, Antioxidants attenuate myocyte apoptosis and improve cardiac function in heart failure: association with changes in the MAPK pathways, Am. J. Physiol. Heart Circ. Physiol. 285 (2003) H822–H832.
[35] G.Z. Feuerstein, P.R. Young, Apoptosis in cardiac diseases: stress- and mitogen-activated signaling pathways, Cardiovasc. Res. 45 (2000) 560–569.
[36] S.A. Cook, P.H. Sugden, A. Clerk, Activation of c-Jun N-terminal kinases and p38-mitogen-activated protein kinases in human heart failure secondary to ischaemic heart disease, J. Mol. Cell. Cardiol. 31 (1999) 1429–1434.
[37] C. Communal, W.S. Colucci, A. Remondino, D.B. Sawyer, J.D. Port, S.E. Wichman, M.R. Bristow, K. Singh, Reciprocal modulation of mitogen-activated protein kinases and mitogen-activated protein kinase phosphatase 1 and 2 in failing human myocardium, J. Card. Fail. 8 (2002) 86–92.
[38] M. Haneda, T. Sugimoto, R. Kikkawa, Mitogen-activated protein kinase phosphatase: a negative regulator of the mitogen-activated protein kinase cascade, Eur. J. Pharmacol. 365 (1999) 1–7.
[39] Q. Liu, P.A. Hofmann, Protein phosphatase 2A-mediated cross-talk between p38 MAPK and ERK in apoptosis of cardiac myocytes, Am. J. Physiol. Heart Circ. Physiol. 286 (2004) H2204–H2212.
[40] R. von Harsdorf, P.F. Li, R. Dietz, Signaling pathways in reactive oxygen species-induced cardiomyocyte apoptosis, Circulation 99 (1999) 2934–2941.
[41] P. Rosini, G. De Chiara, M. Lucibello, E. Garaci, F. Cozzolino, M. Torcia, NGF withdrawal induces apoptosis in CESS B cell line through p38 MAPK activation and Bcl-2 phosphorylation, Biochem. Biophys. Res. Commun. 278 (2000) 753–759.
[42] Y. Ishikawa, E. Kusaka, Y. Enokido, T. Ikeuchi, H. Hatanaka, Regulation of Bax translocation through phosphorylation at Ser-70 of Bcl-2 by MAP kinase in NO-induced neuronal apoptosis, Mol. Cell. Neurosci. 24 (2003) 451–459.
[43] R.A. Kaiser, O.F. Bueno, D.J. Lips, P.A. Doevendans, F. Jones, T.F. Kimball, J.D. Molkentin, Targeted inhibition of p38 mitogen-activated protein kinase antagonizes cardiac injury and cell death following ischemia–reperfusion in vivo, J. Biol. Chem. 279 (2004) 15524–15530.
[44] W.S. Choi, D.S. Eom, B.S. Han, W.K. Kim, B.H. Han, E.J. Choi, T.H. Oh, G.J. Markelonis, J.W. Cho, Y.J. Oh, Phosphorylation of p38 MAPK induced by oxidative stress is linked to activation of both

caspase-8- and-9-mediated apoptotic pathways in dopaminergic neurons, J. Biol. Chem. 279 (2004) 20451–20460.
[45] P. Anversa, G. Olivetti, J.M. Capasso, Cellular basis of ventricular remodeling after myocardial infarction, Am. J. Cardiol. 68 (1991) 7D–16D.
[46] C.A. Beltrami, N. Fianto, M. Rocco, G.A. Feruglio, C. Puricelli, E. Cigola, F. Quaini, E.H. Sonnenblick, G. Olivetti, P. Anversa, Structural basis of end-stage failure in ischemic cardiomyopathy in humans, Circulation 89 (1994) 151–163.
[47] Y.Z. Zhu, Y.C. Zhu, Z.J. Wang, Q. Lu, H.S. Lee, T. Unger, Time-dependent apoptotic development and pro-apoptotic genes expression in rat heart after myocardial infarction, Jpn. J. Pharmacol. 86 (2001) 355–358.
[48] A. Abbate, G.G. Biondi-Zoccai, R. Bussani, A. Dobrina, D. Camilot, F. Feroce, R. Rossiello, F. Baldi, F. Silvestri, L.M. Biasucci, A. Baldi, Increased myocardial apoptosis in patients with unfavorable left ventricular remodeling and early symptomatic post-infarction heart failure, J. Am. Coll. Cardiol. 41 (2003) 753–760.
[49] O. Akyurek, N. Akyurek, T. Sayin, I. Dincer, B. Berkalp, G. Akyol, M. Ozenci, D. Oral, Association between the severity of heart failure and the susceptibility of myocytes to apoptosis in patients with idiopathic dilated cardiomyopathy, Int. J. Cardiol. 80 (2001) 29–36.
[50] Y. Chandrashekhar, S. Sen, R. Anway, A. Shuros, I. Anand, Long-term caspase inhibition ameliorates apoptosis, reduces myocardial troponin-I cleavage, protects left ventricular function, and attenuates remodeling in rats with myocardial infarction, J. Am. Coll. Cardiol. 43 (2004) 295–301.
[51] S. Frantz, A. Ducharme, D. Sawyer, L.E. Rohde, L. Kobzik, R. Fukazawa, D. Tracey, H. Allen, R.T. Lee, R.A. Kelly, Targeted deletion of caspase-1 reduces early mortality and left ventricular dilatation following myocardial infarction, J. Mol. Cell. Cardiol. 35 (2003) 685–694.